Ionic conduction, structural and optical properties of LiCoO2 compound

Ichrak Ben Slima, Karim Karoui, Abdallah Ben Rhaiem

Ionic conduction, structural and optical properties of LiCoO2 compound

ACCEPTED MANUSCRIPT

Ionic conduction, structural and optical properties of LiCoO2 compound

ACCEPTED MANUSCRIPT

Ionic conduction, structural and optical properties of $LiCoO_2$ compound

Ichrak ben slima[a], Karim karoui[a,b] and Abdallah Ben Rhaiem[a]

[a]Laboratory of spectroscopic and optical characterizations of materials, Faculty of Sciences of Sfax, B.P. 1171, 3000 Sfax, University of Sfax, Tunisia.

[b]Greman UMR 7347-CNRS, CEA, INSACVL, University of Tours, Blois, France

Corresponding author: karouikarim36@yahoo.com

Tel:0021625648756

Abstract

$LiCoO_2$ was synthesized by the conventional solid-state reaction. The x-ray diffraction indicates that the $LiCoO_2$ sample crystallize in hexagonal system with R-3m space group. The optical properties were studied. The band gap energy was established and seems to be equal to 2.15eV which confirms the semiconductor character of this compound. The study of the refractive index and the extinction coefficient proved the connection between the sample transparency and a low optical absorption loss. Furthermore, thermal analysis shows an exothermic peak at 335K which was proven by studying the temperature dependence of the electrical properties. The equivalent circuit was chosen and the electrical conductivity was analyzed. The AC conductivities values (10^{-4} $\Omega^{-1}cm^{-1}$) confirm the semiconductor character and the ionic conduction type. The conductions mechanism was attributed to CBH for the first phase and NSPT for the second one. Additionally, electrical modulus investigation reveals the existence of grain boundary and grain effects.

Keywords: Gap energy, refractive index, thermal properties, AC conductivity, CBH/NSPT model.

I. Introduction

Since their commercialization, lithium-ion batteries continuous to receive attention owing to their outstanding performance, such as, high energy density, high specific energy, efficiency, long life, and specific power [1-2]. Divers' electrode materials were investigated including layered transition metal oxides Li_xMO_2, where M is a transition metal, among them, $LiCoO_2$, $LiMnO_2$, $LiFeO_2$, $LiCuO_2$, $LiNiO_2$… [3]. However, the most marketable electrode is $LiCoO_2$ thanks to its good cycling stability and easy production. $LiCoO_2$ batteries have theoretical specific capacity and energy density equal to 274 mAh/g and 1070

ACCEPTED MANUSCRIPT

Wh/kg respectively, while, experimentally, they deliver only half of its theoretical capacity (≈140mAh/g) resulting from structural considerations [4-6].

Moreover, layered transition metal oxides Li_xMO_2 are characterized by their crystalline structure as denoted by Delmas where the alkaline Li occupies an octahedral or prismatic site in 'O' or 'P' structure, respectively [7]. For example, $LiCoO_2$ compound has a layered structure with O3 type (ABCABC). The letter O means that Li^+ ions are free and occupy octahedral sites and the number 3 indicates the sheets number of transition metal in a repeated unit of stacking. Furthermore, $LiCoO_2$ is formed by alternating sheets of CoO_2 with LiO_2. CoO_2 sheets are formed by CoO_6 octahedra sharing faces [8]. These special crystalline structure and the exciting electrochemical results of these materials encourage researchers to study other physical properties for Li_xMO_2 such us optical and electrical properties. For instance, earlier studies on $LiCuO_2$ sample prove that the resistivity of this sample depends on the temperature variation and reaches 10^3 Ω at 300K. The activation energies of this compound vary between 0.1-0.2 eV. This result confirms the semi-conductive behavior of the $LiCuO_2$ sample [9-10]. Moreover, investigation on $LiNiO_2$ indicates that this compound is a small insulator with gap energy equal to 0.4 eV [11]. The activation energies, obtained from electrical analysis, were found to be 0.14; 0.18 and 0.19 eV for z= 0.04; 0.08 and 0.12 respectively, in the $Li_{1-z}Ni_{1+z}O_2$ materials [12]. As well, for $LiFeO_2$, it was proved that this sample is semiconductor with band gap energy equal to 2.4 eV and the activation energy of the temperature dependant conductivity seems to be equal 0.39 eV [13-14]. Recently, a study conducted by R. Bagtache and coworkers, tackling the physical properties of $LiMnO_2$, reveals that $LiMnO_2$ is a semiconductor material with 1.92 eV gap energy value and a conduction process thermally activated with activation energy equal to 0.68 eV [15]. Therefore, from one hand, based on this literary study of alternative $LiMO_2$, from the other hand, based on the electronic properties of $LiCoO_2$ sample which are derived from the electronic configuration of its constituents, where the valence electron states are as following Li ($2s^1$), Co ($3d^7$, $4s^2$) and O ($2s^2$, $2p^4$), we can assume that $LiCoO_2$ sample seems to be attractive as semiconductor. Furthermore, the presences of Li^+ ions free permit the Li^+ ions to be faster which enhances the ionic conductivity and the presence of $Co^{3+/4+}$ in the double valence states estimate a good electronic conductivity [16]. To the best of our knowledge, the study of the optical constants and the temperature dependence of the electrical and dielectric properties as well as the investigation of the conduction mechanism of $LiCoO_2$ compound are not well attempted.

ACCEPTED MANUSCRIPT

From these perspectives, the aim of the present investigation is to study the structural, optical constants, including refractive index and extinction coefficient, and the temperature dependences of the electrical and dielectric properties of the $LiCoO_2$ sample in order to show the higher performance of this material in the semiconductor application domain.

II. Material and method

We used the conventional solid-state reaction to synthesis the $LiCoO_2$ compound. The Li_2CO_3 (Segma Aldrich, 99%) and Co_3O_4 (Segma Aldrich, 99%) were mixed in proportional ratios. The obtained powder was submitted to a first thermal treatment at 623 K for 24h in order to release the CO_2 gas. Then we verified the gas emission by checking the loss of the weight. Finally, the sintering process was at 1023 K for 16 h.

The sample purity was done using the X-Ray Diffraction on powder by 'Siemens D5000' at room temperature with Cu K_α radiation (λ = 1.5406 Å, $10° \leq 2\theta \leq 80°$).

Furthermore, the UV-visible spectroscopy, using 'UV-3101PC' allows investigation optical properties in the wave length domain [200nm-800nm].

Additionally, thermal study was investigated by Differential Scanning Calorimetry (DSC) in the temperature range [300K-550K] with a heating rate 5°/min.

Finally, electrical measurements were carried out on a pellet with 8 mm in diameter and 1 mm in thickness, using the complex impedance spectroscopy 'Solartron1260' in the frequency range [10^{-1}Hz-10^{6}Hz] at various temperatures. To obtain the good contact, pellets were covered on the opposite surfaces with thin layer of silver and mounted between two copper electrodes in a special holder. The powder was pressed by a 5 t/cm^2 pressure in order to acquire a circular disc with 8 mm in diameter and 1 mm in thickness.

III. Result and discussion

III.1. Structural characterization: X-ray Diffraction

XRD allows the identification of the purity of the synthesized compound. The XRD pattern of $LiCoO_2$ is highlighted in Fig.1. The FullProf software was used, by the Rietveld method, for the structural refinements of the prepared sample. It proves that the $LiCoO_2$samplecrystallize in hexagonal system with R-3m space group. The unit cell parameters and the fit criteria are reported in table 1. However, we found a trace of Co_3O_4 corresponding to small peak appearing in the XRD diffractogram.

ACCEPTED MANUSCRIPT

The crystalline structure of the $LiCoO_2$ sample, using Diamond software, is shown in fig.2. This structure is characterized by alternating sheets of CoO_2 layers with layers of free Li^+ ion. The sheets arrangement suggests that this crystalline structure is of O3. Furthermore, CoO_2 sheets are composed by CoO_6 octahedra sharing faces between them. The interatomic distances Co-O equals 2.009 Å and Li-O equal 2Å. The atomics positions are reported in table 2. Although, the advantage of this structure is that the lithium ions are free; this facilitates their mobility and enhances, therefore, the electrical conductivity.

III.2. Optical properties: UV-visible spectroscopy

In order to investigate the optical properties, we use the UV-visible spectroscopy in absorbance mode. Fig.3 displays the absorbance spectrum of the $LiCoO_2$ sample at room temperature. This spectrum is characterized by a strong absorption in the visible domain. The high absorption in the visible range is a favorable criterion for several activity fields such as optoelectronic, photo-catalysis materials and photovoltaic solar cells which allows the $LiCoO_2$ sample to be a candidate for such applications [17-19]. Furthermore, we notice the presence of two absorption peaks. The first peak at 222nm had low intensity and can be attributed to the transition between energy levels in the same bands or energy levels in the band gap [20]. The second peak at 350 nm present a maximum of intensity and corresponds to the transition from the valence band to the conduction band [21-22]. Accordingly, we can get idea about the width of the band gap by direct extrapolation of the absorbance spectra as illustrated in **fig.3** where the intercept of the band corresponding to the transition valence band to the conduction band with the energy axis is equal to 569nm which reflect a gap energy around 2.17eV [23, 24].

In order to comfirm the estimated value of the optical gap energy obtained above, the model proposed by Tauc was used and the E_g is related to the absorption coefficient α by the following relationship [25]:

✔h● ● h● ✔g) r (1)

where ✔ = 2,303*A/e [26], B is a constant, E_g is the optical gap, r is a constant describing the nature of the optical transition between the valence band and the conduction band. In our case, the most intense peak in the absorbance spectrum corresponding to the transition from the valence band to the conduction band is located in the ultra-violet domain, which proves, based on literature study that the transition is of the direct type [27].

ACCEPTED MANUSCRIPT

The value of the gap energy can be defined from the intersection of the extrapolation of the linear part of (✔ h●) ^{2} with the energy axis. The gap energy of the $LiCoO_2$ compound is equal to 2.15 eV which allows classifying this material within the family of semiconductor (fig.4). This gap energy value confirms the one obtained early using the absorbance spectra. The gap energy of $LiCoO_2$ is close to the gap energy of $LiFeO_2$ which equal to 2.4 eV [13].

The extinction coefficient k is calculated based on the following relation [28]:

$$k = \frac{\alpha\lambda}{4\pi} \qquad (2)$$

The evolution of the extinction coefficient k vs. the wavelength □ is shown in Fig.5. It displays small value between 10^{-7} and 10^{-6} which confirms that the $LiCoO_2$ compound possess a low optical absorption loss when the incident light propagates through the crystal which confirms the sample's transparency [29-30].

The refractive index n is calculated based on reflectivity R measurements following [28]:

$$n = \frac{1 + \sqrt{R}}{1 - \sqrt{R}} \qquad (3)$$

The refractive index varies between 2 and 2.8 (fig.6) and its evolution vs. the wavelength ✦ is used to evaluate the Cauchy's constants (n_0, A and B).

The Cauchy's formula of refractive index n is [31]:

$$n = n_0 + \frac{A}{\lambda^2} + \frac{B}{\lambda^4} \qquad (4)$$

The computed values of the Cauchy's constants are determined by fitting the curve of n (✦) are the following: n_0=2.1567; A= -0.0148 µm^{-2}and B= 0.0067µm^{-4}. Thus, in the transparency region of the material, the coefficient B is negligible. Furthermore, these values are close to those previously reported in literature of the $NaCoPO_4$ sample, which are the following: ✔-$NaCoPO_4$ (n_0=2.672; A= -0.028µm^{-2}; B=0.038µm^{-4}); 🚲-$NaCoPO_4$ (n_0=2.276; A=-0.653µm^{-2}; B=0.044µm^{-4}) and ■-$NaCoPO_4$ (n_0=2.116; A=-0.352µm^{-2}; B=0.086µm^{-4}) [31]. These results demonstrate that the wavelength ✦ has no effect on the index n in this material.

III.3. Differential Scanning Calorimetry (DSC)

In order to study the phase transitions existing in the material, differential scanning calorimetry (DSC) was used. The thermogram of the $LiCoO_2$ compound, shown in fig.7, is in the temperature range from 300K to 550K and with a heating rate of 5°/min. Two peaks are present. From one side, the first peak is exothermic and intense observed at 335K, and

ACCEPTED MANUSCRIPT

provided the enthalpy ΔH= 11.31 kJ/mol and the entropy ΔS= 33.76 J/(mol K). This allows classifying this transition as an order–disorder type [32]. From the other side, the second peak is endothermic observed at 500K. It may be due to the decomposition of the material. However, the transition at 335Kcould be detected by the electrical properties when varying temperature.

III.4. Electrical properties

III.4.1. electrical impedance spectroscopy

Fig.8 displays the Nyquist diagrams of the compound $LiCoO_2$. These spectra are distinguished by the existence of two distinct frequency domains: high, and low frequencies, according to the grain effect and the grain boundary effect, respectively. Furthermore, the conduction process in $LiCoO_2$sample is thermally activated which is indicated by the drop in the - Z'' vs. Z' of the arc-circle of Nyquist spectrum and the shift towards higher frequencies while temperature rises.

To better understand the different contributions in this material we have tried to found an equivalent circuit that describes the behavior of this material using Z-View software. The choice of the equivalent circuit was based on the best fit between the experimental and theoretical curves with the smallest errors. The good fit between the experimental and theoretical data was found using a circuit formed by two cells connected in series: the first cell is composed of a resistance R, a capacitor C and a fractal capacitor CPE connected in parallel, while the second cell is composed of a resistance R and a fractal capacitor CPE connected in parallel (Fig.8). The all parameters of resistance and capacity of the grain and grain boundaries response are grouped in the table 4.

The resistance values deduced from the equivalent circuit at each temperature are used to calculate the conductivity of the grain based on the following relationship [33]:

$$\sigma_g = \frac{e}{RS} \qquad (5)$$

Where: e is the thickness of the pellet, S is the surface area of the pellet and R is the resistance.

The variation of grain conductivity as a function of the inverse of temperature is illustrated in Fig.9. This variation follows Arrhenius law:

ACCEPTED MANUSCRIPT

$$\sigma_g = \sigma_0 \exp\left(-\frac{E_a}{K_B T}\right) \quad (6)$$

The evolution of grain conductivity shows a discontinuity at temperature T= 338K. This is confirmed by the result of the differential scanning calorimetry analysis (DSC). The activation energies of two phases are E_a= 0.16 eV for phase I and E_a= 0.38 eV for phase II.

III.4.2. AC conductivity

The variation of the AC conductivity of the $LiCoO_2$, at several temperatures, is illustrated in Fig.10. This variation shows that the AC conductivity remains almost constant at low frequencies and undergoes dispersion at high frequencies, which is a characteristic of ω^s. We also notice the low values of the σ_{ac} conductivity which is of the order of 10^{-4} to $10^{-3}\,\Omega^{-1}cm^{-1}$ which confirms the conductive character of this material. This result of the electrical conductivity of the $LiCoO_2$ sample ($10^{-3}\,\Omega^{-1}cm^{-1}$) is close to the electrical conductivity of the layered $LiFeO_2$ ($1.9\ 10^{-3}\,\Omega^{-1}cm^{-1}$ at 373k) [14]. While, by comparing the electrical conductivity of the $LiCoO_2$ sample ($10^{-3}\,\Omega^{-1}cm^{-1}$) with this of the $LiFePO_4$ ($10^{-9}\,\Omega^{-1}cm^{-1}$) we note that the $LiFePO_4$ has a poor electrical conductivity [34]. This result highlights the importance of the crystalline structure in the conductivity mechanism. While the Li^+ ions in $LiCoO_2$ are free, the Li^+ ion in $LiFePO_4$ is confined in LiO_6 octahedra and linked to the FeO_6 octahedra and PO_4 tetrahedra [35]. As a result, the electronic – ionic conductivity is affected by the crystalline structure which shows the important role of the free Li^+ ion in the conduction within this material.

The modeling of the experimental conductivity data has been carried out following the law of Jonscher [36]:

$$\sigma_{ac}(\omega) = \sigma_{dc} + A\omega^s \quad (7)$$

Where, σ_{ac} is the alternating current conductivity, $\sigma_{dc}$is the direct current conductivity, A is a constant and s the exponent that represents the degree of interaction between the carriers of mobile ions and the environments around them.

The adjustment of the conductivity spectra using the Jonscher equation shows a good agreement between the experimental and theoretical spectra (Fig.10) and makes it possible to determine the σ_{dc} and the exponent s.

The logarithmic variation of the conductivity dc as a function of the inverse of the temperature is shown in fig.11.This variation is described by Arrhenius' law:

$$\sigma_{dc} = \sigma_0 \exp\left(-E_a/K_B T\right) \quad (8)$$

ACCEPTED MANUSCRIPT

A change in slope at temperature 342K is marked which is approved by the calorimetric study. The linear adjustment of the slopes allows us to deduce the values of the activation energies associated with the DC conduction of the two phases. The obtained values are equal to 0.11 eV for the first phase and 0.36 eV for the second phase. Noting that, these values are close for those found earlier in the evolution of grain conductivity.

Based on Elliot's theory [37], we can determine the mechanisms of conduction in each phase using the variation of the exponent s which translates the interaction between movable ions and their environments. The variation of the exponent s as a function of temperature is recorded in fig.12.This variation shows that above 330K the exponent s decreases when the temperature increases, which means that the conduction of the material at its own is described by the correlated barrier hopping model (CBH). While below 330K, the exponent s shows an increase as the temperature rises, indicating that small polaron tunnel (NSPT) model.

III.4.3. Electrical modulus

The electrical modulus is used to study the relaxation process in a sample. It was calculated using the following equation:

$$M'' = \omega C_0 Z' (\omega, \rho) \qquad (9)$$

Fig 13 highlights the imaginary parts of the electric modulus of the $LiCoO_2$ sample. We notice the presence of two relaxations; the first one, at low frequency, associated with the grain boundary effect and the second one, at high frequency, correspond to the grains effect. These two relaxations shift toward high frequencies with the increase of the temperature which indicates that the relaxation process is thermally activated.

The simulation of these spectra was done using Bergman equation [38-39]:

$$M'' = M''_{1max}/((1 - \beta_1) + (\beta_1/(1 + \beta_1)))[\omega_{1max}/\omega + (\omega/\omega_{1max})\beta_1] + [M''_{2max}/((1 - \beta_2) + (\beta_2/(1 + \beta_2)))[(\omega_{2max}/\omega) + (\omega/\omega_{1max})\beta_2] \qquad (10)$$

Where ω_{max} is the frequency corresponding to the maximum modulus M", β reflects the extent of coupling between the mobile ions in the conduction process and vary in the range (0-1). The logarithmic evolution of the frequency ω_{max} relative to M''_{max}as a function of the inverse of temperature is displayed in fig 14. This evolution follows the Arrhenius law:

$$\omega_{max} = \omega_0 \exp(-E_a/K_B T) \qquad (11)$$

ACCEPTED MANUSCRIPT

We note the presence of a slope changing at 340 K confirming the phase transition observed by the thermal study. The obtained activation energies are equal to 0.19 eV for phase I and 0.33 eV for phase II.

Conclusion

The $LiCoO_2$ sample was synthesized using solid state method. The structural refinement, using XRD, proves that this sample crystallize in hexagonal system with R-3m space group. Furthermore, optical investigation reveals that this sample is a semiconductor with width band gap equal to 2.15 eV. Additionally, the study of the refractive index and the extinction coefficient confirms the sample transparency with low absorption loss. Thermal study of the prepared sample was carried out using DSC measurements and indicates a phase transition at 335 K. This phase transition was detected by the ac conductivity analysis which corroborates the CBH model for the first phase and the NSPT model for the second one. The study of the electrical modulus reveals the presence of grain boundary and grain effects.

References:

[1]. Horiba, T. (2014). Lithium-ion battery systems. *Proceedings of the IEEE*, *102*(6), 939-950.

[2]. Nitta, N., Wu, F., Lee, J. T., & Yushin, G. (2015). Li-ion battery materials: present and future. *Materials Today*, *18*(5), 252-264.

[3]. Xu, B., Qian, D., Wang, Z., & Meng, Y. S. (2012). Recent progress in cathode materials research for advanced lithium ion batteries. *Materials Science and Engineering: R: Reports*, *73*(5-6), 51-65.

[4]. Lyu, Y., Wu, X., Wang, K., Feng, Z., Cheng, T., Liu, Y., & Guo, B. (2021). An overview on the advances of $LiCoO_2$ cathodes for lithium-ion batteries. *Advanced Energy Materials*, *11*(2), 2000982.

[5]. Rao, M. C., & Hussain, O. M. (2009, July). Optical and electrical properties of laser ablated amorphous $LiCoO_2$ thin film cathodes. In *IOP Conference Series: Materials Science and Engineering* (Vol. 2, No. 1, p. 012037). IOP Publishing.

[6]. Zhou, A., Wang, W., Liu, Q., Wang, Y., Yao, X., Qing, F., & Li, J. (2017). Stable, fast and high-energy-density $LiCoO_2$ cathode at high operation voltage enabled by glassy B_2O_3 modification. *Journal of Power Sources*, 139*362*, 131.

ACCEPTED MANUSCRIPT

[7]. Delmas, C., Fouassier, C., & Hagenmuller, P. (1980). Structural classification and properties of the layered oxides. *Physica B+ C*, *99*(1-4), 81-85.

[8]. Gabrisch, H., Yazami, R., & Fultz, B. (2002). The character of dislocations in $LiCoO_2$. *Electrochemical and Solid-State Letters*, *5*(6), A111.

[9]. Owens, F. J. (1999). Evidence of a phase transition in Cu–O chains of $LiCuO_2$. *Physica C: Superconductivity*, *313*(1-2), 65-69.

[10]. Utsumi, W., Imai, K., Koike, M., Takei, H., Yagi, T., Takahashi, H., & Môri, N. (1993). Pressure effect on the crystal structure and electrical conductivity of $LiCuO_2$. *Journal of Solid State Chemistry*, *107*(2), 507-512.

[11]. Anisimov, V. I., Zaanen, J., & Andersen, O. K. (1991). Band theory and Mott insulators: Hubbard U instead of Stoner I. *Physical Review B*, *44*(3), 943.

[12]. Molenda, J., Wilk, P., & Marzec, J. (2002). Structural, electrical and electrochemical properties of $LiNiO_2$. *Solid State Ionics*, *146*(1-2), 73-79.

[13]. Tangra, A. K., & Lotey, G. S. (2021). Synthesis and investigation of structural, optical, magnetic, and biocompatibility properties of nanoferrites $AFeO_2$. *Current Applied Physics*, *27*, 103-116.

[14]. Rosaiah, P., & M Hussain, O. (2013). Synthesis, electrical and dielectrical properties of lithium iron oxide. *Advanced Materials Letters*, *4*(4), 288-295.

[15]. Bagtache, R., Brahimi, R., Abdmeziem, K., & Trari, M. (2019). Physical properties of o-$LiMnO_2$. *Applied Physics A*, *125*, 1-4.

[16]. Molenda, J. (2011). Li-ion batteries for electric vehicles. In *Annales Universitatis Mariae Curie-Sklodowska* (Vol. 66, p. 23). Maria Curie-Skłodowska University

[17]. Harrabi, D., Hcini, S., Dhahri, J., Wederni, M. A., Alshehri, A. H., Mallah, A., & Bouazizi, M. L. (2022). Study of Structural and Optical Properties of Cu–Cr Substituted Mg–Co Spinel Ferrites for Optoelectronic Applications. *Journal of Inorganic and Organometallic Polymers and Materials*, 1-14.

[18]. Wang, J., Zhang, C., Liu, H., McLaughlin, R., Zhai, Y., Vardeny, S. R., &Vardeny, Z. V. (2019). Spin-optoelectronic devices based on hybrid organic-inorganic trihalide perovskites. *Nature Communications*, *10*(1), 1-6.

[19]. Kalthoum, R., Bechir, M. B., &Rhaiem, A. B. (2020). $CH_3NH_3CdCl_3$: A promising new lead-free hybrid organic–inorganic perovskite for photovoltaic applications. *Physica E: Low-Dimensional Systems and Nanostructures*, *124*, 114235.

ACCEPTED MANUSCRIPT

[20]. Jellibi, A., Chaabane, I., &Guidara, K. (2016). Spectroscopic ellipsometry and UV–vis studies at room temperature of the novel organic–inorganic hybrid of salt Bis (4-acetylanilinium) tetrachlorocadmiate. *Physica E: Low-Dimensional Systems and Nanostructures*, *79*, 167-172.

[21]. Farhadi, S., Javanmard, M., &Nadri, G. (2016). Characterization of cobalt oxide nanoparticles prepared by the thermal decomposition. *Acta Chimica Slovenica*, *63*(2), 335-343.

[22]. Taghavimoghaddam, J., Knowles, G. P., & Chaffee, A. L. (2012). Preparation and characterization of mesoporous silica supported cobalt oxide as a catalyst for the oxidation of cyclohexanol. *Journal of Molecular Catalysis A: Chemical*, *358*, 79-88.

[23]. López, R., & Gómez, R. (2012). Band-gap energy estimation from diffuse reflectance measurements on sol–gel and commercial TiO_2: a comparative study. *Journal of Sol-Gel Science and Technology*, *61*, 1-7.

[24]. Tauc, J. (1968). Optical properties and electronic structure of amorphous Ge and Si. *Materials Research Bulletin*, *3*(1), 37-46.

[25]. Trabelsi, K., Karoui, K., Hajlaoui, F., Zaghrioui, M., Jomni, F., & Rhaiem, A. B. (2022). An organic-inorganic hybrid cadmium chloride with face-sharing $CdCl_6$ octahedral chains: Synthesis, crystal structure, optical and conduction mechanisms: $[NH_2(CH_3)_2]_5Cd_3C_{l1}$. *Optical Materials*, *134*, 113100.

[26]. Soliman, T. S., & Vshivkov, S. A. (2019). Effect of Fe nanoparticles on the structure and optical properties of polyvinyl alcohol nanocomposite films. *Journal of Non-Crystalline Solids*, *519*, 119452.

[27]. Sui, Yan, et al. "A Semiconducting Organic–Inorganic Hybrid Metal Halide with Switchable Dielectric and High Phase Transition Temperature." *The Journal of Physical Chemistry C* 123.14 (2019): 9364-9370.

[28]. Mahfoudh, N., Karoui, K., & BenRhaiem, A. (2021). Optical studies and dielectric response of $[DMA]_2MCl_4$ (M= Zn and Co) and $[DMA]_2ZnBr_4$. *RSC Advances*, *11*(40), 24526-24535.

[29]. Lakhdar, M. H., Larbi, T., Ouni, B., &Amlouk, M. (2013). Optical and structural investigations on Sb_2S_2O new kermesite alloy for optoelectronic applications. *Journal of Alloys and Compounds*, *579*, 198-204.

[30]. Wemple, S. H., & DiDomenico Jr, M. (1971). Behavior of the electronic dielectric constant in covalent and ionic materials. *Physical Review B*, *3*(4), 1338.

ACCEPTED MANUSCRIPT

[31]. Ajmi, A., Karoui, K., Khirouni, K., &Rhaiem, A. B. (2019). Optical and dielectric properties of $NaCoPO_4$ in the three phases α, β and γ. *RSC Advances*, *9*(26), 14772-14781.

[32]. Mahfoudh, N., Karoui, K., Gargouri, M., &BenRhaiem, A. (2020). Optical and electrical properties and conduction mechanism of $[(CH_3)_2NH_2]_2CoCl_4$. *Applied Organometallic Chemistry*, *34*(3), e5404.

[33]. Slima, I. B., Karoui, K., Mahmoud, A., Boschini, F., &Rhaiem, A. B. (2022). Effects of Mn doping on structural properties and conduction mechanism of $NaCu_{0.2}Fe_{0.8-x}Mn_xO_2$ (x= 0.4; 0.5; 0.6; 0.7) materials. *Journal of Alloys and Compounds*, *920*, 166002.

[34]. Ban, C., Yin, W. J., Tang, H., Wei, S. H., Yan, Y., & Dillon, A. C. (2012). A novel codoping approach for enhancing the performance of $LiFePO_4$ cathodes. *Advanced Energy Materials*, *2*(8), 1028-1032.

[35]. Zhang, W. J. (2011). Structure and performance of $LiFePO_4$ cathode materials: A review. *Journal of Power Sources*, *196*(6), 2962-2970.

[36]. Slima, I. B., Karoui, K., Mahmoud, A., Boschini, F., &Rhaiem, A. B. (2022). Structural, optical, electric and dielectric characterization of a $NaCu_{0.2}Fe_{0.3}Mn_{0.5}O_2$ compound. *RSC Advances*, *12*(3), 1563-1570.

[37]. Trabelsi, K., Karoui, K., Jomni, F., &Rhaiem, A. B. (2021). Optical and AC conductivity behavior of sodium orthosilicate Na_2CoSiO_4. *Journal of Alloys and Compounds*, *867*, 159099.

[38]. Rathan, S. V., &Govindaraj, G. (2010). Electrical relaxation studies on $Na_2NbMP_3O_{12}$ (M= Zn, Cd, Pb and Cu) phosphate glasses. *Materials Chemistry and Physics*, *120*(2-3), 255-262.

[39]. Bergman, R. (2000). General susceptibility functions for relaxations in disordered systems. *Journal of Applied Physics*, *88*(3), 1356-1365.

ACCEPTED MANUSCRIPT

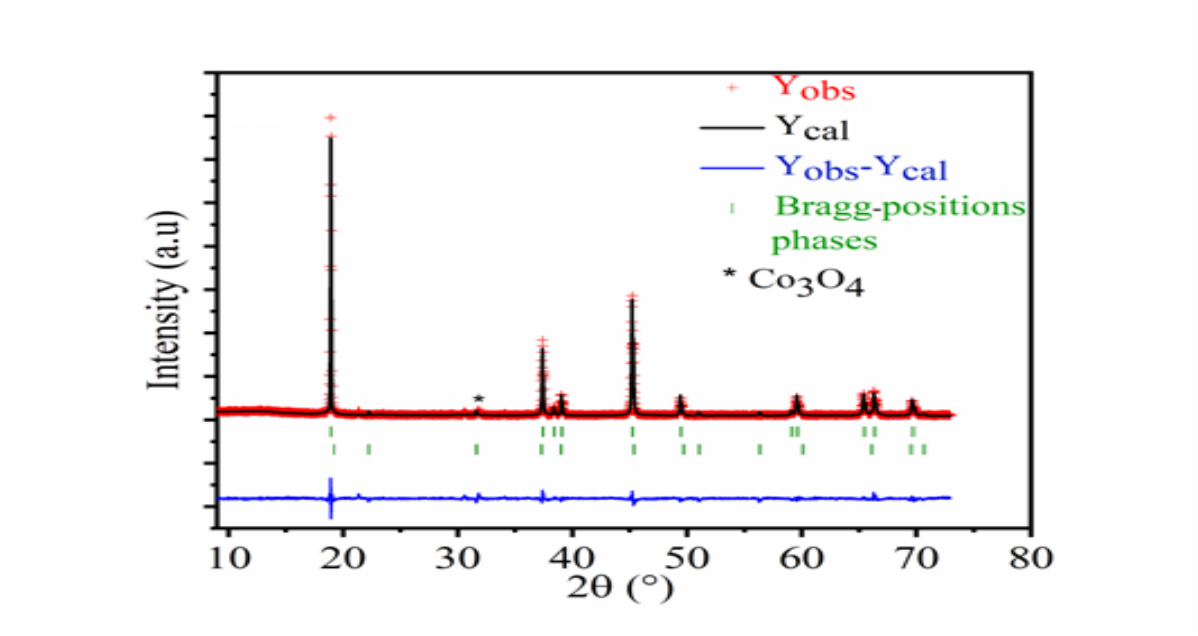

Figure 1:XRD pattern of $LiCoO_2$

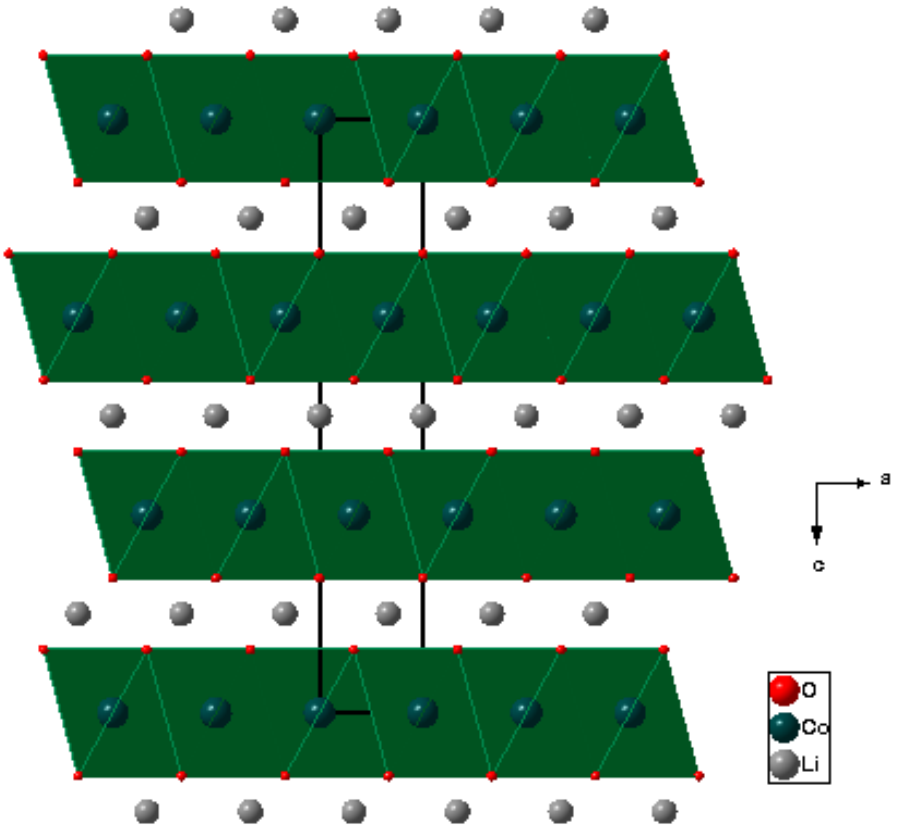

Figure 2 : crystalline structure of $LiCoO_2$

ACCEPTED MANUSCRIPT

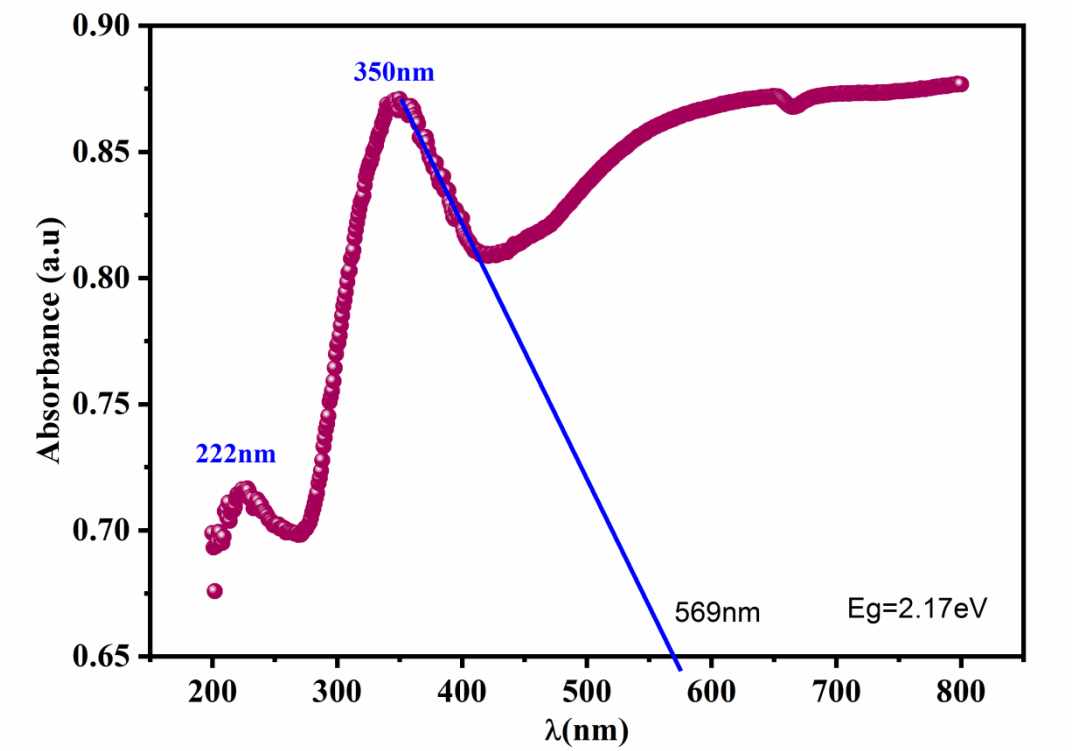

Figure 3 : Uv-visible absorbance spectra and estimation of the gap energy of $LiCoO_2$.

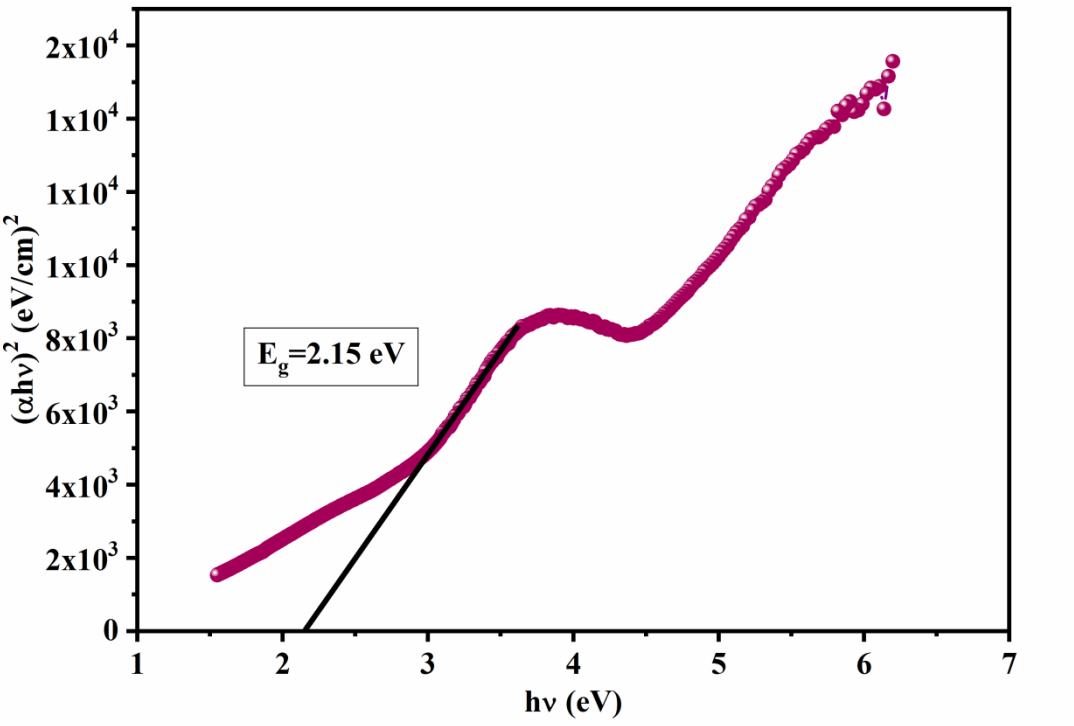

Figure 4 :(✔ h●)^{2}plotof $LiCoO_2$

ACCEPTED MANUSCRIPT

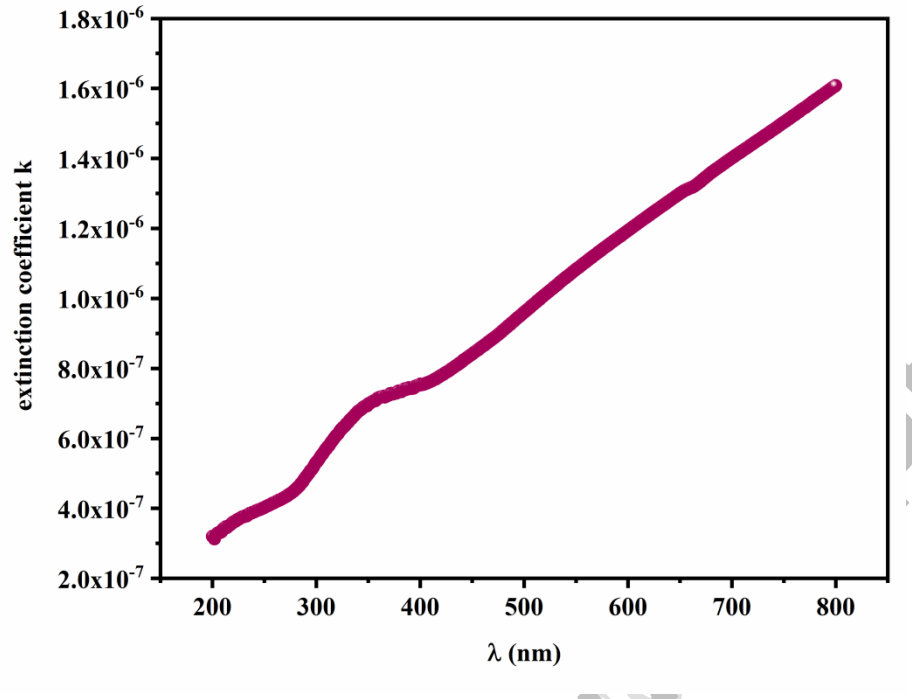

Figure 5 : extinction coefficientof $LiCoO_2$

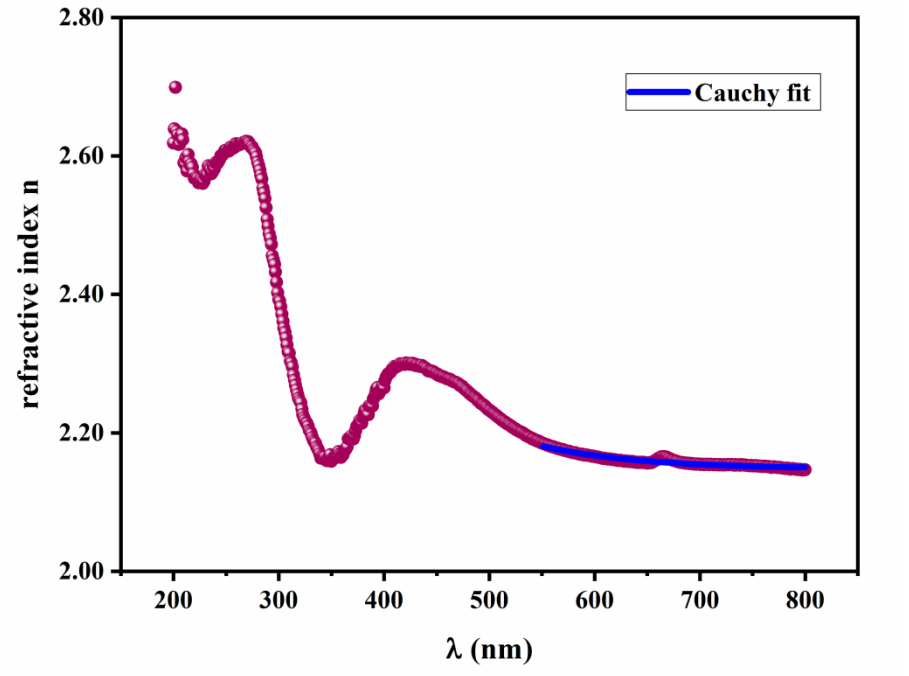

Figure 6 : refractive indexof $LiCoO_2$

ACCEPTED MANUSCRIPT

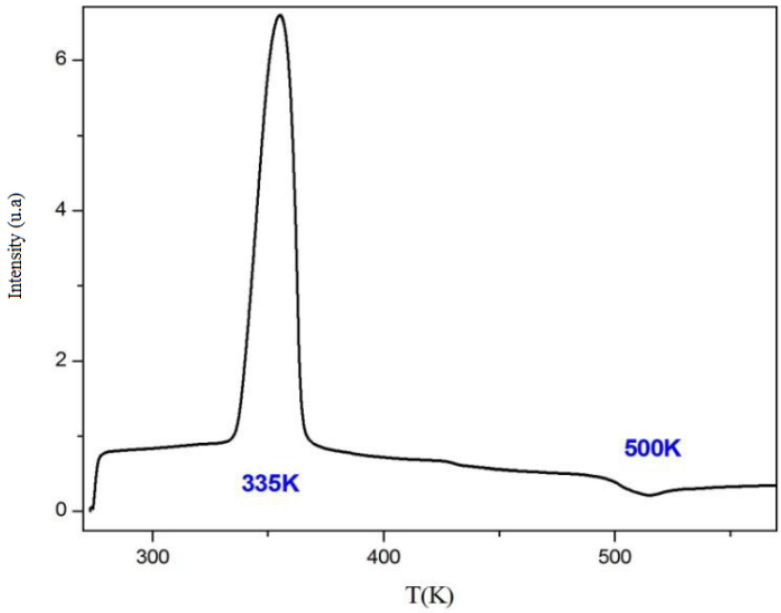

Figure 7 : thermogram of $LiCoO_2$

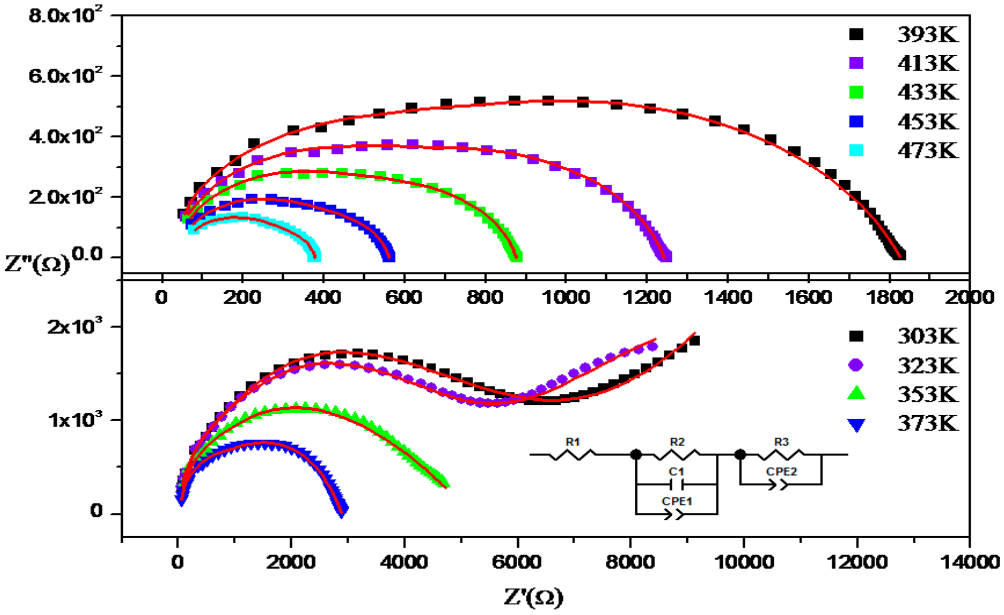

Figure 8: Nyquist diagram of $LiCoO_2$

ACCEPTED MANUSCRIPT

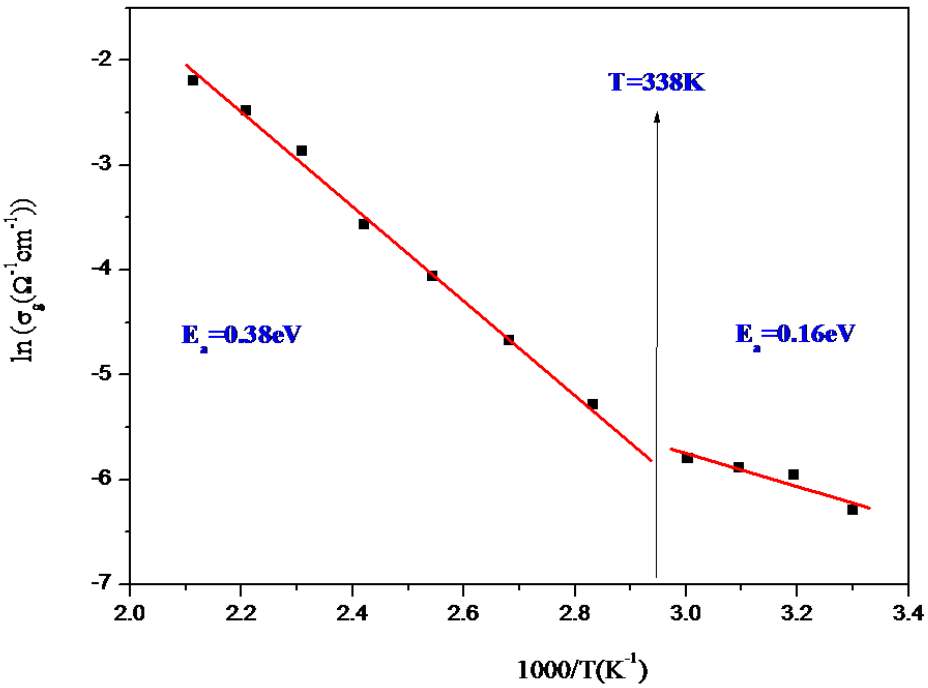

Figure 9: Grain conductivity of $LiCoO_2$

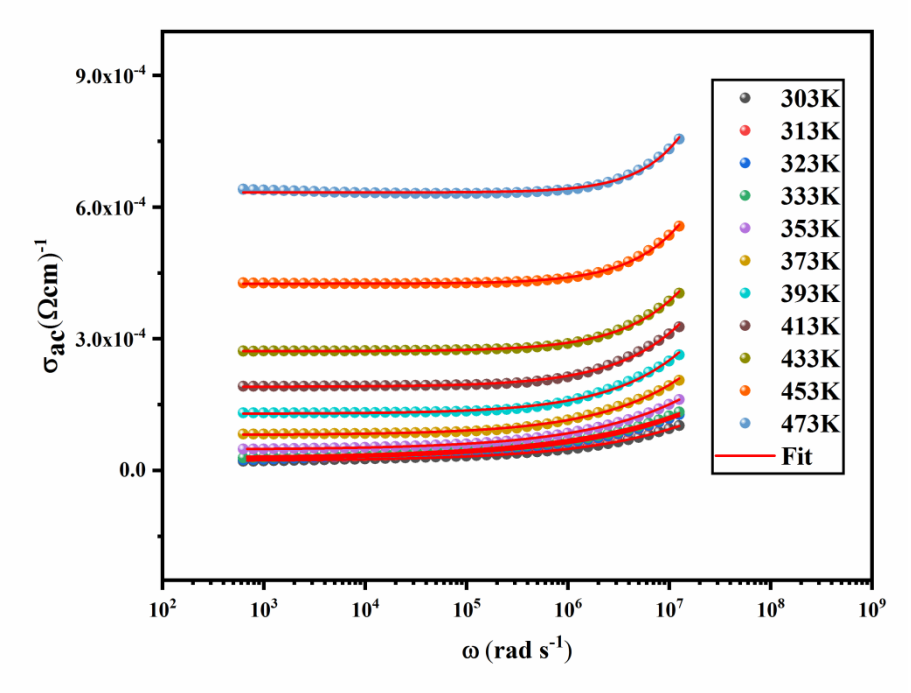

Figure 10 : AC conductivity of $LiCoO_2$

ACCEPTED MANUSCRIPT

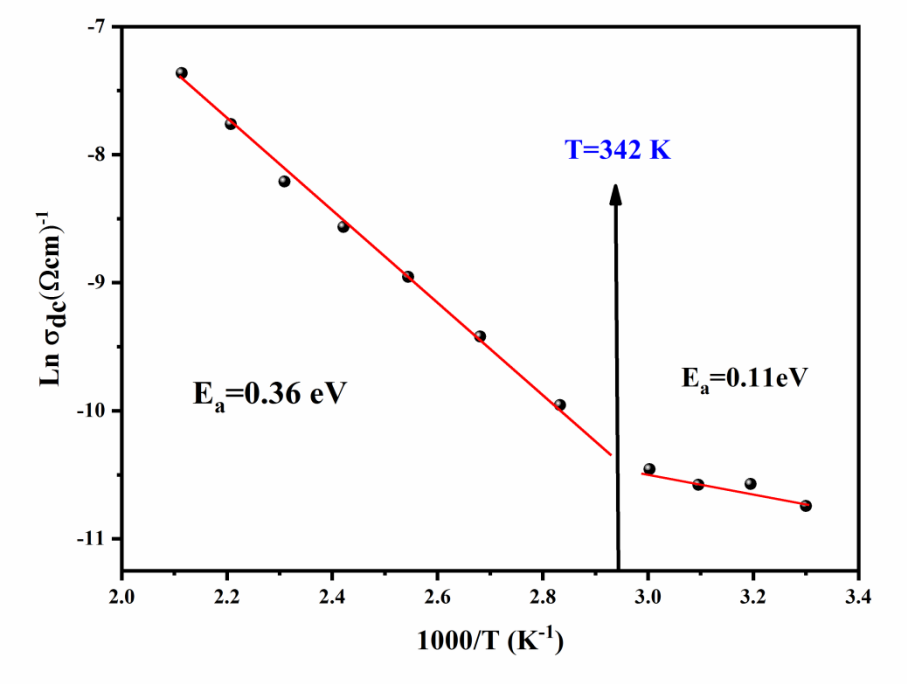

Figure 11: DC conductivity of $LiCoO_2$

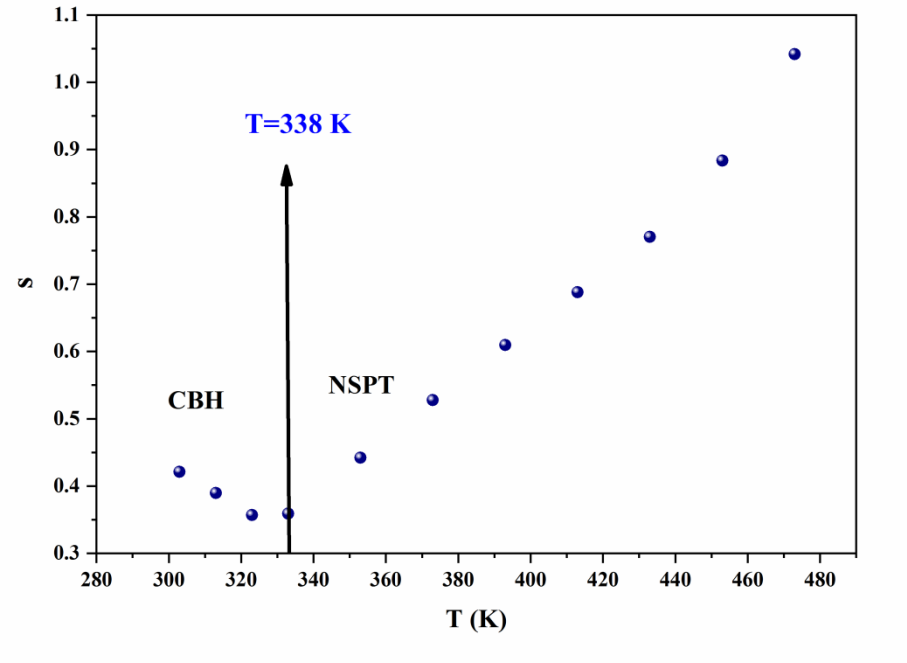

Figure 12 : Variation of the exponent sof $LiCoO_2$

ACCEPTED MANUSCRIPT

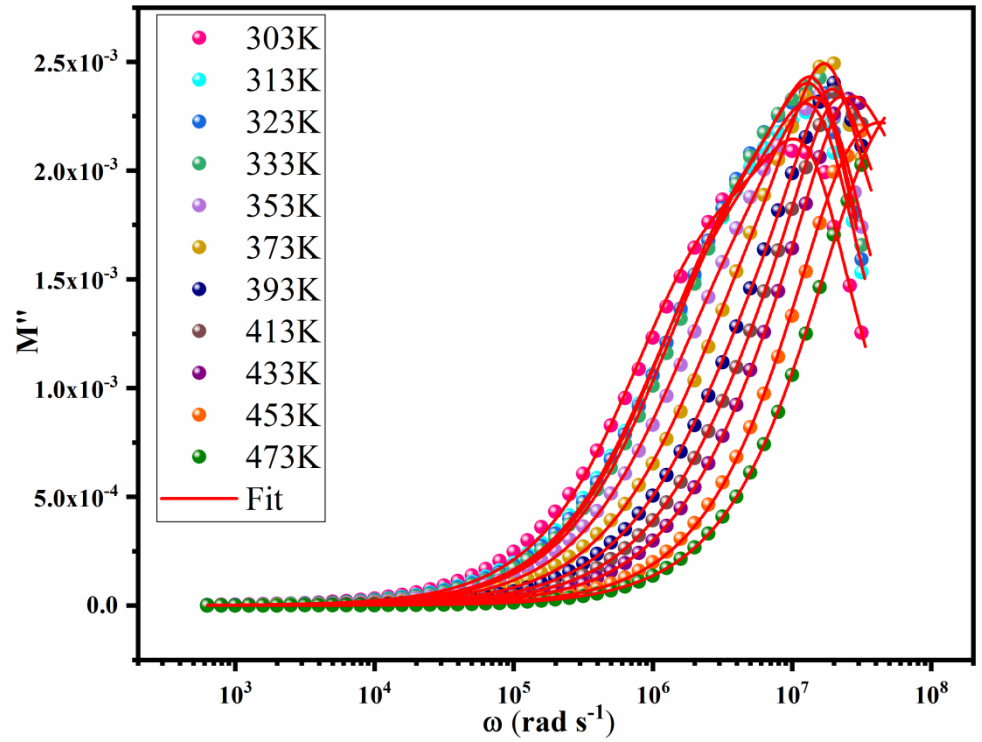

Figure 13 : Evolution of the imaginary part of the electric modulus of $LiCoO_2$

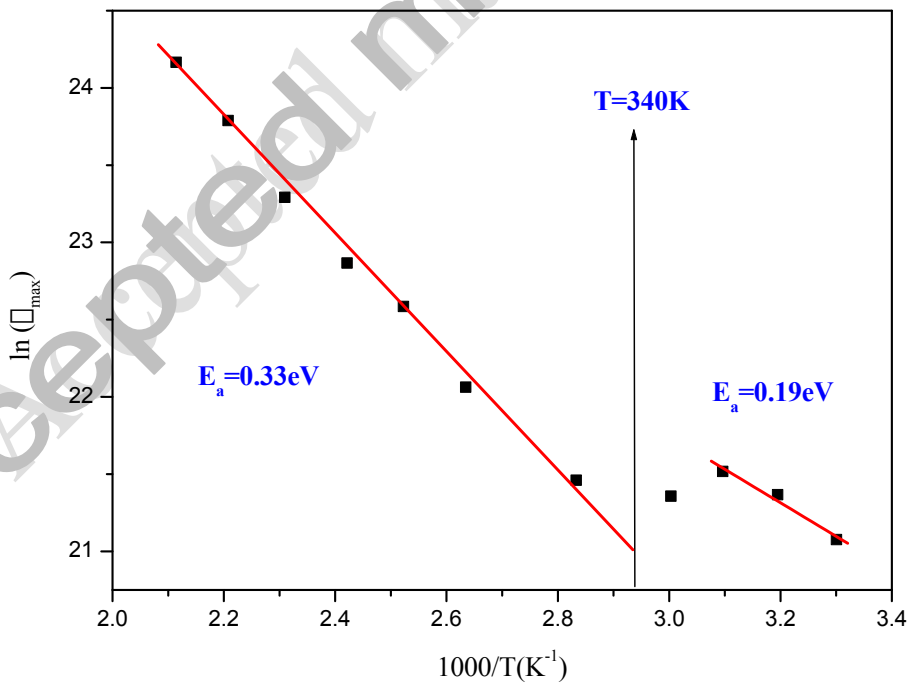

Figure 14: Evolution of $\ln \tau_{max}$ vs. the temperature of $LiCoO_2$ sample.

ACCEPTED MANUSCRIPT

Table 1 : unit cell parameters and fit criteria of $LiCoO_2$

$LiCoO_2$	
Crystal system	Hexagonal
Space group	R-3m
Formula units (Å)	a=b= 2.8168(5) c=14.0614(6) α=β=90 □=120
Volume (Å^3)	96.62
Space group	R-3m
R_p(%)	35.7
R_{wp}(%)	29.9
R_{exp}(%)	17.50
□ ^{2}	2.92
R_B(%)	4.221
R_F(%)	2.616

Table 2 : crystalline structure parameters of $LiCoO_2$

Atom	Wyck.	x	y	z	U
O1	6*c*	0	0	0.2631(4)	0.0000
Co1	3*a*	0	0	0	0.0000
Li1	3*b*	0	0	½	0.0000

Table 3 : Cauchy parameters of $LiCoO_2$

Paramètres	n_0	A (µm^{-2})	B (µm^{-4})
$LiCoO_2$	2.15677	0.014825	**0.0067139**

ACCEPTED MANUSCRIPT

Table 4 : equivalent circuit parameters of the Nyquist diagrams of $LiCoO_2$

T(K)	R_g(▶)	C_g(F)	CPE_g(F)	R_{jg}(▶)	CPE_{jg}(F)
303	8256	2,0964E-8	1,213E-10	11467	1,3061E-6
313	6484.59	4,6656E-10	1,425E-11	10586	1,2634E-6
323	6285	3,91E-10	2,012E-11	6747	4,7815E-6
333	5181,21	3,3772E-10	4,939E-11	5894	4,4654E-7
353	3242,01	1,132E-9	5,125E-11	4741	2,1191E-7
373	1537,33	1,787E-9	7,524E-11	2362	5,1244E-7
393	829,8	2,059E-9	1,243E-10	1331	5,7821E-7
413	463,7	2,475E-9	1,425E-10	878,6	6,7715E-7
433	226,39	2,928E-9	1,833E-10	575,4	4,6749E-6
453	131,69	3,008E-9	2,128E-10	370,5	8,0858E-6
473	83,92	4,514E-9	2,378E-10	253,8	6,698E-7